First-principles calculations of size-dependent giant electroresistance effect in nanoscale asymmetric ferroelectric tunnel junctions

Xin Luo, Yue Zheng', and Biao Wang'

Citation: Journal of Applied Physics **111**, 074102 (2012); doi: 10.1063/1.3698503
View online: http://dx.doi.org/10.1063/1.3698503
View Table of Contents: http://aip.scitation.org/toc/jap/111/7
Published by the American Institute of Physics

First-principles calculations of size-dependent giant electroresistance effect in nanoscale asymmetric ferroelectric tunnel junctions

Xin Luo,[1,2] Yue Zheng,[1,a)] and Biao Wang[1,b)]
[1]*State Key Laboratory of Optoelectronic Materials and Technologies/Institute of Optoelectronic and Functional Composite Materials, and Micro & Nano Physcis and Mechanics Research Laboratory, School of Physics and Engineering, Sun Yat-sen University, Guangzhou 510275, China*
[2]*Institute of High Performance Computing, 1 Fusionopolis Way, #16-16 Connexis, Singapore 138632, Singapore*

(Received 6 October 2011; accepted 25 February 2012; published online 3 April 2012)

Based on the first principle calculations, we predicted the electronic structures and ferroelectric instability of the asymmetric ferroelectric tunneling junction with the ferroelectric barrier thickness changing, and found two undiscovered and important behaviors, i.e., absence of the critical thickness for the positive polarization state and the larger critical thickness for the negative polarization state. Using nonequilibrium Green function's approach, the corresponding two-probe systems and their electronic transport properties at different ferroelectric barrier thickness have been constructed. It is found that reorienting the polarization direction in the ferroelectric barrier can dramatically change the internal electric field and macroscopic potential barrier, resulting in several orders of magnitude change in tunneling electroresistance ratio. Results also found that the tunneling electroresistance can be distinctly controlled by adjusting thickness of the ferroelectric barrier, which behavior is defined as the size-dependent giant electroresistance effect. Our results enable architectures of large density and high sensitivity in the next generation of ferroelectric random access memories with nondestructive resistive readout. © *2012 American Institute of Physics*. [http://dx.doi.org/10.1063/1.3698503]

I. INTRODUCTION

Ferroelectric materials have attracted a lot of attention during the past few decades, for reasons of both scientific curiosity and prospects of practical industry applications. Of particular interests are their application in the data storage, in recent years, the ferroelectric random access memory (FRAM) have emerged as an alternative to traditional magnetic and nonpolar dielectric based memory[1,2] for the nonvolatile digital information storage. FRAM is a promising technology for nonvolatile application because it has many outstanding features: ultralow power consumption (power usage is about 99% lower than dynamic random access memory), faster writing performance (the response of polarization to an external field is within 1 ns), and a much greater maximum number of write-erase cycles. Recently, memory density of up to a terabit per square inch has been obtained[3,4] in the nanoscale ferroelectric tunnel junctions (FTJ)[5,6] or capacitors, the key elements of FRAM. For example, Lee *et al.*[3] have used a bottom-up patterning approach to fabricate ultrahigh density (about 176 Gb in.$^{-2}$) ferroelectric memories in the form of a series of individual FTJ arrays. However, in the present FRAM, the major difficulties are still coming from the size limitation. It is not clear how small the FRAM can be scaled to maintain its polarization and ferroelectricity. On the other hand, reducing the basic cell size may cause the data signal to become too weak to be detectable. In order to advance the further developments of FRAM, it is necessary to elucidate the basic physical problems in the FTJ structures, and look for some new mechanisms to shed light on the design of new architecture.

As the ferroelectricity is a collective phenomenon, for a long time it is commonly believed that there is a critical thickness, below which the ferroelectricity or spontaneous polarization in FTJ will be suppressed due to effects of the surfaces, interfaces and uncompensated depolarization field.[7] Based on the first principle calculations, Junquera *et al.*[8] used the frozen phonon methods predicted that ultrathin single domain $BaTiO_3$ films between conducting $SrRuO_3$ electrodes lose ferroelectricity below the thickness of 6 unit cells. Considering the relaxation of atoms at the interfaces, Tagantsev *et al.*[9] found that the critical thickness of the $SrRuO_3$/$BaTiO_3$/$SrRuO_3$ heterostructures is further reduced to 3 unit cells (12 Å). At the same time, many experimental studies also found that the ferroelectricity can only be retained above some critical thickness of about 1–10 nm.[10–12] In addition, Fong *et al.*[13] and Aguado *et al.*[14] indicated that the formation of domain structures can even stabilize the ferroelectricity in films with a thickness of 2 unit cells, which is also the minimum bulk ferroelectric environment size (~8 Å). The existence of ferroelectricity in nanometer-thick FTJ has led to renewed interest in exploring the ferroelectrics in applications of the electronic nanodevices.[15,16]

One of the prominent features in ferroelectrics is the strong coupling of the spontaneous polarization and external fields.[17–19] Experimentally, it has been observed that the Curie temperature and polarization state will be greatly enhanced with the application of the compressive epitaxial strain.[20] It is well known that the spontaneous polarization

a)Electronic mail: zhengy35@mail.sysu.edu.cn.
b)Electronic mail: wangbiao@mail.sysu.edu.cn.

in the ferroelectric barrier can be switched by the applied electric field, which results in the different charge distribution at electrode/ferroelectric interfaces. For an asymmetric FTJ (A-FTJ), it will cause a significant different internal electrostatic potential profiles across the junction. As proposed by Tsymbal *et al*. and Kohlstedt *et al*. in the continual models based on the thermodynamic and classic quantum mechanical theories,[21–23] the tunneling electroresistance (TER) across ferroelectric barrier can vary significantly in A-FTJ when the spontaneous polarization is reversal. Recent experiments[14,15,24] have directly detected evidence for ferroelectricity-related giant electroresistance (GER) effect in A-FTJ with a ultrathin ferroelectric barrier.

Since in the ultrathin FTJ structures with a barrier thickness of a few nanometers, the quantum effects are dominant, and many detailed mechanisms are related to the internal atomic movements and their thickness. Therefore a microscopic quantum mechanical method is required to further elucidate the effect of polarization switching on the electron transport properties of A-FTJ in an atomic scenario. In this work, we perform *Ab-initio* density functional theory calculations on a $Pt/BaTiO_3/SrRuO_3$ A-FTJ with variable ferroelectric barrier thickness. This choice is motivated that $SrRuO_3$ is a suitable oxide electrode for the epitaxial growth due to its similar lattice with the substrate and $BaTiO_3$, and Pt is a well conductive metal electrode. Their combination will cause greater asymmetric in both interface of the FTJ. Here, we are particularly interested in the size-dependent ferroelectric instabilities and their influences on electron transport properties and GER effect of the A-FTJ.

II. METHODOLOGY

In order to get an accurate relaxed ground state of these large heterostructures, we perform density functional theory (DFT) calculations using the Vienna Ab Initio Simulation Package (VASP).[25] Our theoretical calculations are based on DFT within the local density approximation (LDA). A plane-wave basis set and projector augmented wave (PAW)[26] potentials as implemented in VASP are employed. In the energy calculation, we have used a well converged $8 \times 8 \times 1$ Monkhorst-Pack grid for k-point sampling in the Brillouin zone of the tetragonal cell, together with a 0.2 eV Gaussian broadening. The plane-wave energy cutoff was set to 500 eV. During the structural relaxation, the ion positions and the out of plane lattice constants were then relaxed with the constraint that the in-plane lattice constants were fixed to the theoretical value of $SrTiO_3$ substrate. The configurations were considered as relaxed until the maximum Hellman-Feynman force acting on each atom was less than 0.01 eV/Å. Based on these fully relaxed structures, the electronic and ferroelectric properties are calculated. The "short-circuit" boundary conditions, equivalent to a metallic contact of top and bottom electrode layers, are imposed by the periodically repeated superlattice structure.[7]

For the electron transport properties, the conductance of the FTJ are explored by the Atomistix ToolKit (ATK),[27] which is based on nonequilibrium Green's function (NEGF) combined with density functional theory (DFT). The above $Pt/BaTiO_3/SrRuO_3$ relaxed structures were used to construct the scattering region, and the periodicity of the supercell in the transport directions was replaced by two semi-infinite electrodes. Thus, the constructed two probe systems are embedded in the Pt and $SrRuO_3$ electrodes. The valence electrons are expanded in a numerical atomic-orbital basis set of single ξ plus polarization (SZP) for all atoms. Perdew-Zunger local density approximation (LDA) is adopted for exchange-correlation. In order to get converged results of the conductance, we used a dense k-point mesh of 50×50 to sample in the surface two-dimensional Brillouin zone for the two-probe calculation. All the calculated parameters are tested to result in good convergence.

The atomic structures, electronic properties and electroresistance of the asymmetric $Pt/BaTiO_3/SrRuO_3$ tunneling junction are obtained by the first-principle calculations and nonequilibrium Green function's approach.

III. RESULTS AND DISCUSSION

A. Size-dependent ferroelectric stabilization of A-FTJ

In our calculations, the simulation supercell is built up by aligning the (001) oriented $BaTiO_3$ ferroelectric films with the Pt (001) and $SrRuO_3$ (001) electrodes. The $BaTiO_3$ has two different interfacial terminations: with $BaO\text{-}Pt_2$ terminated type for the Pt electrodes and TiO_2-SrO terminated type for the $SrRuO_3$ electrodes. In such asymmetric interfacial structures, the effective screening lengths λ_{eff} are estimated to be 0.202 and 0.003 Å for TiO_2-SrO and $BaO\text{-}Pt_2$ heterointerfaces,[28] respectively. The large contrast of the effective screening lengths at both dissimilar interfaces is a necessary condition to produce the giant tunneling electroresistance (TER) due to their dominant influence on the average potential barrier height.[21,22] We consider an example of A-FTJ epitaxially grown on a (001) cubic $SrTiO_3$ substrate, which is a typical substrate to grow atomically well defined ferroelectric thin film. Therefore, the in-plane lattice constant is fixed to be $a = 3.866$ Å (the *ab initio* calculated value of lattice parameter of the cubic $SrTiO_3$), which is smaller than the theoretical lattice constant of tetragonal $BaTiO_3$ (3.946 Å) and the electrodes. As a result, the lattice mismatch between A-FTJ and substrate produce substantial tetragonal distortions in $BaTiO_3$ ($c/a = 1.064$) and electrodes. The imposed compressive strain of 2.07% for $BaTiO_3$ in the A-FTJ will greatly enhanced the polarization. In practice, this large misfit strain is available in very thin films epitaxially grown on substrate.[29] For instance, Garcia *et al*.[14] have experimentally demonstrated that a large compressive strain of up to 3% can be achieved in ferroelectric thin film with a thickness of 3 nm. On the other hand, the large in-plane compressive epitaxial strain will also increase the ferroelectric phase transition temperature[12,16] and favor the polarization in *c* phase[30] (i.e., $P_x = P_y = 0, P_z \neq 0$).

The basic unit cell of the $Pt/BaTiO_3/SrRuO_3$ tunneling junction has a generic formula: $(Pt_2)_6/(BaO\text{-}TiO_2)_m/(SrO\text{-}RuO_2)_3$, where *m* stands for the number of $BaTiO_3$ unit cell. The different thickness of the ferroelectric tunnel barriers is monitored by changing *m* from 2 to 9 unit cells. In each thickness, we start with an out of plane ferroelectric displacement obtained from the bulk $BaTiO_3$ ferroelectrics in

the junction barrier and then fully relaxed. The relaxed atomic structure of $Pt/BaTiO_3/SrRuO_3$ FTJ with $m = 5$ $BaTiO_3$ barrier layer for the two opposite polarization directions are shown in the insert of Fig. 1. We designated the junction with a polarization P_{up} pointing toward $SrRuO_3$ as A-FTJ_1, and the one with opposite polarization P_{down} pointing toward Pt electrode is designated as A-FTJ_2. Figure 1 shows the relative Ti-O displacements within each TiO_2 monolayer in $BaTiO_3$ unit cells for different thickness. It is found that the A-FTJ_1, i.e., the spontaneous polarization pointing to SRO electrode, is only stable above the thickness of $m = 5$ unit cells (~2 nm). For example, with an initial A-FTJ_1 structure in the $m = 4$ unit cells junction, the polarization will flip into the A-FTJ_2 state after relaxation with the spontaneous polarization pointing toward the Pt electrode. When increasing $BaTiO_3$ barrier thickness, the net polarization of A-FTJ_1 is enhanced and approached a stable value at the thickness of 3.2 nm ($m = 7$). On the other hand, for A-FTJ_2 with 1 nm ($m = 2$) barrier thickness, there is still a large displacements between Ti cation and the center of oxygen octahedral cage, indicating a stable ferroelectric phase in monodomain configuration. The existence of ferroelectricity in the minimum bulk environment thickness indicates that the critical thickness is practically absent in the A-FTJ_2. Moreover, it is found that the Ti-O displacements within each TiO_2 monolayer are distributed inhomogeneous across the barrier. These results mean that the distribution of the polarization in ferroelectric barrier is also inhomogeneous due to effect of asymmetric surfaces and interfaces.

For the $BaTiO_3$ bulk material in tetragonal phase, the energy gain is equivalent when the spontaneous polarization pointing up or down along the c axis. Therefore, all the odd ranks of Landau free energy expansion are absent, and the curves of free energy versus electric displacements exhibit a symmetric double potential well profile. However, the appearance of electric field breaks up the symmetric double well, producing shallow and deep potential well.[31] For our asymmetric ferroelectric tunnel junctions, the A-FTJ_1 is located at the shallow well while A-FTJ_2 is in the deep well, as shown in Fig. 2(a). The behaviors of the two junction structures can be understood by examining the total internal electric field, which is composed of the built in electric field E_{bi} and the residual depolarizing field E_d in our system. Note that, the built in electric field is resulted from the different work function of both the electrodes and termination of the ferroelectrics. Since the work function of (001) $SrRuO_3$ and clean Pt surface is found to be 5.2 eV (Ref. 32) and 5.75 eV,[33] respectively, there is a large contact potential difference that contributed to the built in electric field E_{bi}, as is indicated by Fig. 2(b). For the ferroelectric state thin film, the bounded polarized charges will appear at the electrode/ferroelectric interface and produced the bounded charge depolarization field E_{cd}. In response to the E_{cd}, the free electrons in the electrode will move to the boundary area to screen the bounded charge, and the redistribution of the screen charge will induce the screening electric field E_{sc}. Due to the incomplete screening of electrodes, the final residual depolarizing field E_d is the combination of the bounded charge depolarization field E_{cd} and screening electric field E_{sc}. The depolarizing field E_d points to the opposite direction of the spontaneous polarization. The schematic band diagram of A-FTJ_1 structure is illustrated in Fig. 2(c), where E_{bi} and E_d have the same directions. Thus, the overall internal field suppress the polarization in A-FTJ_1 below the thickness of 2 nm ($m = 5$). While for A-FTJ_2, the opposite direction of E_{bi} and E_d produces a cancel effect in the ferroelectrics, and results in a smaller internal field [Fig. 2(d)]. That is why the A-FTJ_2 structure can maintain the ferroelectricity in the minimum thickness ($m = 2$) of bulk ferroelectric environment, it also explains the absence of critical thickness and proves previous discussions about effect of asymmetric interfaces/electrodes on critical properties of A-FTJ.[34,35]

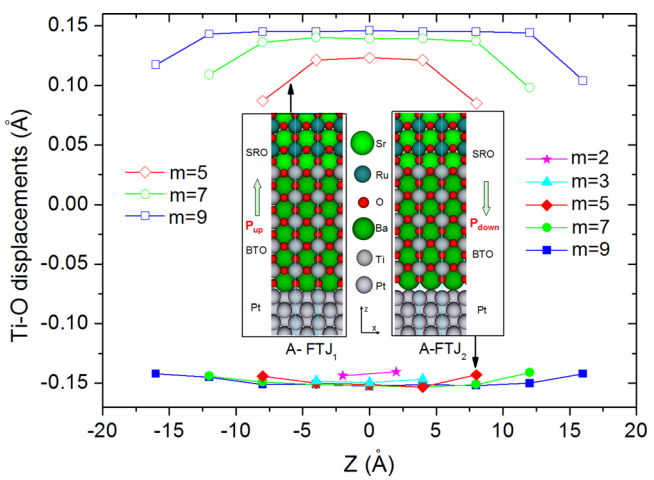

FIG. 1. Relative Ti-O rumpling for A-FTJ. The relative Ti-O rumpling in the ferroelectric $BaTiO_3$ barrier for different thickness. Positive and negative values correspond to the local electric dipole moment pointing toward $SrRuO_3$ and Pt, respectively, as shown in the inserted illustration. The arrows mark the direction of the polarization of $BaTiO_3$.

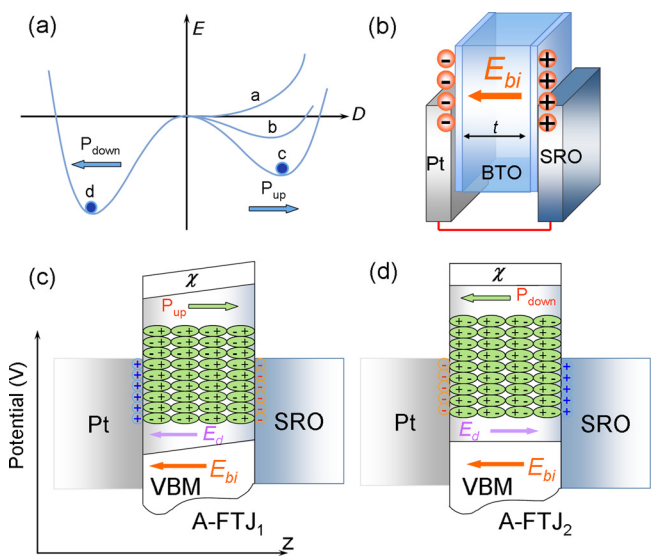

FIG. 2. Schematic potential and electric fields in A-FTJ. (a) Schematic double well potential of the $Pt/BaTiO_3/SrRuO_3$ junctions as a function of the dipole displacements. (b) Charge transfer and the resulting built in electric field E_{bi} due to the different work function of the asymmetry electrodes and interfaces. The simplified band diagram of the asymmetric junction in short circuit boundary condition for (c) A-FTJ_1 and (d) A-FTJ_2, χ is the electron affinity of the insulator, and E_d is the depolarizing field.

Using the density functional perturbation theory,[36] the Born effective charges (Z^*), optical dielectric constants, and piezoelectric tensor are calculated and listed in Table I. The oxygens are located at the face center in the cubic phase, and they have two inequivalent directions to move in the tetragonal phase, either perpendicular or along the Ti-O chain. We designate the oxygen with displacement perpendicular the Ti-O chain as $O_\perp$, and those with displacement along the Ti-O chain as $O_\parallel$. The results of the Z^* in cubic phase are in good agreement with previous calculations.[37,38] However, as the tetragonal distortion increase, the absolute values of Z^* in Ti and O are decreasing in the ferroelectric phase. It is possible that the tetragonal distortion of the crystal field induced by elongation of the TiO_6 octahedra along z-direction leads to a Jann-Teller stabilization of the orbitals. Since the $d(z^2)$ orbital of Ti is further away from the oxygens, the energy is lower as Ti is repelled less by the oxygen ligands, and the Z^* is smaller as a result of the change in orbital mixing. A similar trend is also found in the optical electric constants, the polar distortions tend to decrease ε_∞. The experimental value of polarization $P_s = 0.26$ C/m^2 is slightly less than our calculated value of 0.307 C/m^2. Compared to the theoretical value of free bulk ferroelectrics, the epitaxial strain can greatly enhance the polarization and reach 0.396 C/m^2 for the $BaTiO_3$ on $SrTiO_3$ substrate. From the calculated Z^* and the ionic displacements relative to their ideal positions, we estimate the polarization of the central unit cell to be 0.34 and 0.37 C/m^2 for A-FTJ_1 and A-FTJ_2 with the barrier thickness of 2.8 nm ($m = 7$). Particularly, we found that the polarizations are almost constant in A-FTJ_2, while they vary from 0.29 to 0.35 C/m^2 in FTJ_1 as the thickness increases from $m = 5$ to $m = 9$ unit cells.

B. Electronic properties and structures in A-FTJ

Presently, the most exciting prospect of FTJ lies in its electronic application. Thus, we focus on the electronic structures and electron transport properties of the A-FTJ. Before proceeding, it is worth noting that the charge transfer between the electrodes and insulating barrier is exacerbated by the underestimated bandgap problem in DFT calculation. The bandgap of the $BaTiO_3$ as computed within LDA (1.6–1.9 eV) is significantly smaller than the experimental gap of 3.2 eV, as shown in Table I. As pointed out by Junquera and Ghosez,[39] this underestimation of bandgap will produce unphysical population of the conduction bands in ferroelectrics when align the bandstructures in the electrode/ferroelectric interfaces. In order to avoid the pathological situations where the Schottky barrier $\phi_n < 0$, we apply a Hubbard U correction to the Ti *3d* states.[40] As a result, the bandgap of $BaTiO_3$ is open up and reach 2.74 eV for our strained ferroelectric in the LDA+U method with U = 7 eV. In the following, we will use this method to investigate the electronic structure in $Pt/BaTiO_3/SrRuO_3$ A-FTJ. Figure 3 shows the local density of states (LDOS) in the $m = 6$ unit cells tunneling junctions, where the solid curves is for the A-FTJ_1 and the blue shaded plots correspond to the LDOS in A-FTJ_2. The Fermi level is indicated by the dash lines. It is clear that the positions of the LDOS in middle ferroelectric layer of A-FTJ_2 are almost the same as those in an ideal strained bulk $BaTiO_3$ with a bandgap of 2.7 eV. While those in A-FTJ_1 move holistically toward negative energy range compared to their ideal bulk counterpart, indicating a strong electric field in the ferroelectric barrier of A-FTJ_1. As a result, the conduction band of A-FTJ_1 is lower with a Schottky barrier of $\phi_{n1}^{LDAU} = 1.05$ eV, which is smaller than that in FTJ_2 ($\phi_{n2}^{LDAU} = 1.95$ eV). By carefully examining the LDOS in each $BaTiO_3$ layer, we found that there is a strong charge transfer from electrodes to the oxides due to the metal induced gap states in the oxide, which is universal in the metal/insulator interface when the Fermi level is located within the bandgap of the insulator. Especially in the first $BaTiO_3$ layer adjacent to the Pt electrode of A-FTJ_1, the filling of the metal induced gap states and interfacial Pt-O bonding, producing a smaller bandgap in the oxide as shown in Fig. 3. Owing to the presence of compensation charge carriers in the ferroelectrics, the traditional Thomas-Fermi screening model should do some modification to account for the more efficient screening mechanism[41] resulted from the enhanced concentration of free charge carriers in the interfacial $BaTiO_3$ layer. From these analyses, it is anticipated that the tunneling electroresistance in A-FTJ_1 will be significantly smaller than that in A-FTJ_2.

C. Size-dependent giant electroresistance of A-FTJ

To obtain the electronic transport properties of the strained A-FTJ, we use the fully self-consistent nonequilibrium Green's function (NEGF) method combined with the DFT calculations. The tunneling conductance of the above

TABLE I. Calculated lattice constants, Born effective charges (|*e*|), electronic dielectric constant, band gap, and spontaneous polarization in $BaTiO_3$ perovskite for the three structures.

$BaTiO_3$	Lattice constants (Å)	Z^*(A)	Z^*(B)	$Z^*(O_\perp)$	$Z^*(O_\parallel)$	ε_∞	E_g (eV)	Polar (C/m^2)
Cubic	$a = 3.954$	+2.76	+7.42	−2.16	−5.84	6.84	LDA = 1.65 LDA + U = 2.52	0
Tetragonal	$a = 3.946$, c/a = 1.011	+2.80	+6.37	−2.03	−5.10	6.49	LDA = 1.80 LDA + U = 2.61	0.307
Tetragonal (strained)	$A = 3.866$, c/a = 1.064	+2.85	+5.27	−1.91	−4.26	6.21	LDA = 1.86 LDA + U = 2.74	0.396
Experimental	Cubic:[b] $a = 3.996$ Tetragonal:[c] $a = 3.991$, c/a = 1.011					5.86[a]	3.2[d]	0.26[e]

[a]Reference 44, measured in ferroelectric phase.
[b]Reference 45, measured at a temperature of 474 K.
[c]Reference 46, measured at the room temperature of 300 K.
[d]Reference 47, obtained from the cubic structure.
[e]Reference 48, measured for the tetragonal structure at the temperature of 297 K.

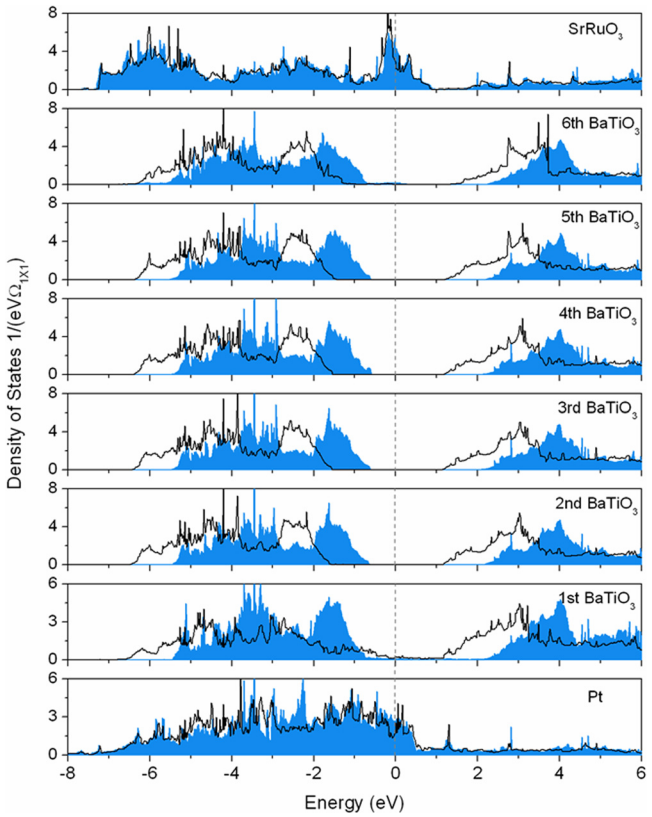

FIG. 3. LDOS of ferroelectric junctions for each layer in the 6 unit cell $BaTiO_3$ and for the interfacial Pt and $SrRuO_3$ unit cell. The solid curves correspond to the LDOS of A-FTJ$_1$, and the shaded plots are the LDOS of A-FTJ$_2$. All the LDOS are calculated within LDA+U (where U = 7 eV) method.

A-FTJ can be expressed by the classical Büttiker formula as,[42,43]

$$G = G_0 \sum_{k_{||}} T(E_F, k_{||}), \tag{1}$$

where G_0 is the conductance quantum, $T(E_F, \boldsymbol{k}_{||})$ is the transmission coefficient at the Fermi energy E_F for a given value of the transverse wave vector $\boldsymbol{k}_{||}$. In general, the overall potential profile $U(z)$ in FTJ can be determined by the properties of two electrodes and the direction of the depolarization field E_d in the polar ferroelectrics.[21,22]

Based on the first principles NEGF-DFT calculations, Fig. 4 shows the calculated tunneling electroresistance of the $Pt/BaTiO_3/SrRuO_3$ junction with respect to a wide range of barrier thickness. It is noted that the resistance is related with conductance by $R = 1/G$. For the FTJ$_1$, the polarization will flip into A-FTJ$_2$ state below the thickness of 2 nm ($m = 5$), thus only the resistance above that thickness is obtained. In consistent with previous LDOS analyses, the tunneling electro-resistance in A-FTJ$_1$ is of orders of magnitude smaller than that in FTJ$_2$. The relative change of the resistance R between the two opposite polarization states in A-FTJ$_1$ and A-FTJ$_2$ is described by the giant electroresistance (GER), which is define as

$$\mathrm{GER} = \frac{R_{\mathrm{A-FTJ_2}} - R_{\mathrm{A-FTJ_1}}}{R_{\mathrm{A-FTJ_1}}} \tag{2}$$

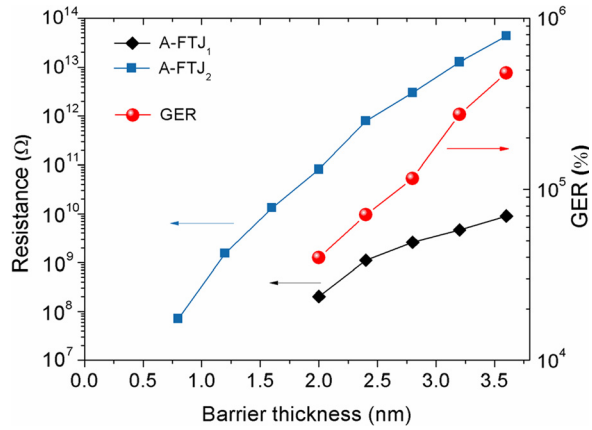

FIG. 4. Size dependent giant electro-resistance in A-FTJ. Calculated electroresistances of the $Pt/BaTiO_3/SrRuO_3$ junctions at different barrier thickness. The A-FTJ$_1$ and A-FTJ$_2$ correspond to the junctions with polarization pointing toward $SrRuO_3$ and Pt, respectively. Giant electroresistance (GER) is the ratio between their resistances.

in our work, where $R_{\mathrm{A-FTJ1}}$ and $R_{\mathrm{A-FTJ2}}$ are the tunneling resistances of A-FTJ$_1$ and A-FTJ$_2$, respectively. It is noted that the GER ratio increases exponentially with barrier thickness, reaching about 140|000% for $t_{\mathrm{BTO}} = 2.8$ nm barrier. These results are in line with the experimental observation of giant tunnel electroresistance in $BaTiO_3/La_{0.66}Sr_{0.33}MnO_3$ bilayers.[14,15] It is predicted that the GER ratio will further enhance with the increase of FTB thickness and is dominated by the potential barriers. The merit of manipulate the tunnel electroresistance by reversing the polarization is apparent in the sensitive readout of FRAM. Since in the traditional FRAM, reading is a destructive process and requires the cell to be rewritten to retain its information when it was changed. The incorporation of the nondestructive readout mechanism will further reduce its power consumption and enhance the sensitivity of signal detection.

With decreasing film thickness, the introduction of metal/ferroelectric interface will produce surface capacitor effects that deteriorate the performance of microscopic ferroelectric devices, as well as give rise to substantial depolarizing field in the ferroelectrics. Due to the strong field about the interface region, both the electrodes and ferroelectrics will have large mechanical ionic relaxation, which in turn causes great modification of the boundary conditions and influence the transport properties.[38] To gain more insight of the interfacial effect on GER, Figs. 5(a) and 5(b) show the relaxed atomic structures and corresponding charge density contours of A-FTJ$_1$ and A-FTJ$_2$ with $m = 6$ unit cells. For both A-FTJ$_1$ and A-FTJ$_2$, comment features are that the Ti ions are shifted away from the center of their respective O octahedral cage to produce the spontaneous polarization. In the A-FTJ$_1$ with the polarization pointing toward $SrRuO_3$ electrode, the ionic relaxations at the BaO/Pt interface show a strong Pt−O bonding character. From the charge density contours of vertical Ti-O plane, it is interesting to note that a compact conductive channel is formed in A-FTJ$_1$ through the connection of the bonding, making the Pt metallic states penetrated through the barrier extensively. On the other hand, for A-FTJ$_2$, the distances between subsurface O ions

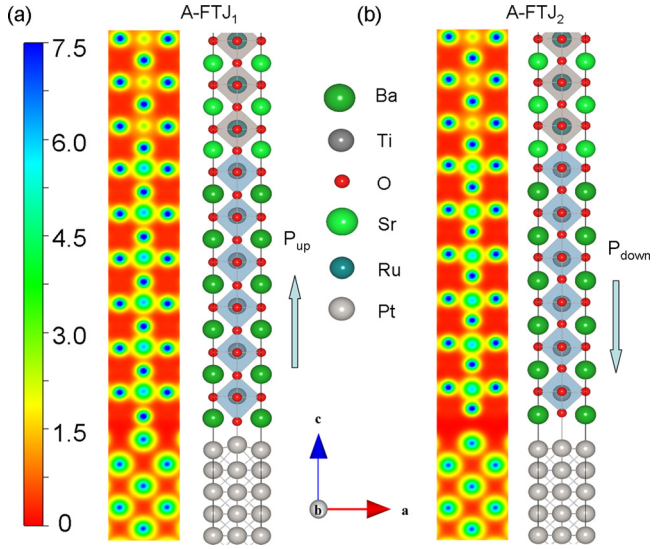

FIG. 5. Charge density profiles in A-FTJ. Charge density profiles along the transport direction for the A-FTJ$_1$ and A-FTJ$_2$. The relaxed atomic structures are shown next to the charge density contour, where the arrows show the directions of the polarizations.

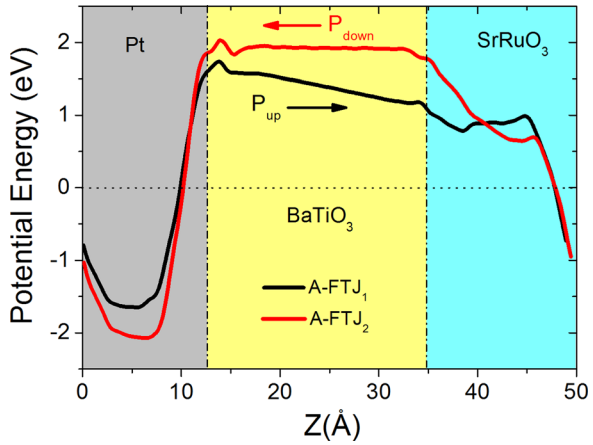

FIG. 6. Electrostatic potential in A-FTJ. Macroscopic averages of the electrostatic potential energy $\bar{V}$ profile of A-FTJ$_1$ (black) and A-FTJ$_2$ (red). The Fermi level is set to zero as reference energy.

and the outmost Pt electrode change by some amounts, which in turn modify the electronic structure dramatically. As is evident in Fig. 5(b), charge density on the interface O and its neighboring Pt are localized in A-FTJ$_2$, and the interfacial separation and rumpling of Pt-O atoms contribute to the high decay rate in the barrier. Much more about the screening mechanism can be extracted from the relaxed junction structures. It is clear that in the first $SrRuO_3$ layer near the interface, the bounded polarization charges in ferroelectrics are penetrated into the oxides electrodes through the relative Ru-O ionic displacement (about 0.03 and 0.08 Å for A-FTJ$_1$ and A-FTJ$_2$, respectively). As a result, the polarizations in ferroelectrics continue for some distance into the metal-oxide electrodes in the form of ionic displacements. This enhanced screening ability can effectively suppress the interfacial capacitor effect and supporting the ferroelectricity in ultrathin ferroelectric films.

Since conductance G of the Pt/$BaTiO_3$/$SrRuO_3$ junction is determined by the effective potential barrier, we have also calculated the potential profile to elucidate the effect of polarization reversal on the GER, as shown in Fig. 6. Based on the first principle simulations, it is found that the average potential barrier height of A-FTJ$_2$ is higher than that of A-FTJ$_1$ due to their different bonding behavior and interfacial rumpling. The value of the average barrier is 1.1 and 1.9 eV with respect to the Fermi level for A-FTJ$_1$ and A-FTJ$_2$, respectively, this result is in consistence with previous LDOS analysis. The unscreened polarization charges in the junctions give rise to a depolarizing field E_d pointing opposite to the polarization. In A-FTJ$_2$, the E_d has the opposite direction with the build in electric field E_{bi}. Due to the similar magnitude of both fields, they cancel out each other in A-FTJ$_2$ as reflected from the flat potential curve. As mentioned previous, E_d and E_{bi} have the same direction in A-FTJ$_1$, and their overall effects produce large internal electric field that will flip the polarization when the ferroelectric barrier thickness below 2 nm. The amplitude of internal field can be deduced from the slope of the macroscopic average potential in FTJ$_1$. Owing to the presence of the electric fields, one of the conduction band minimum (CBM) edge is lowered by 0.45 eV. However, the Fermi level is still located inside the bandgap of $BaTiO_3$. The combined effect of the atomic displacement and internal electric filed behavior give rise to the different potential barrier and produce large GER ratio in A-FTJ.

IV. CONCLUSIONS

To conclude, we have examined structural and electronic transport properties of strained asymmetric Pt/$BaTiO_3$/$SrRuO_3$ tunnel junction with considering effects of ferroelectric barrier thickness, asymmetric interfaces and electrodes. Through the novel design of asymmetric termination and electrodes in A-FTJ, we have shown that the reversal of the spontaneous polarization can produce a large tunnel electroresistance ratio, which is also significantly determined by the ferroelectric barrier thickness. The generation of a large internal field induced by the different work functions of asymmetric electrodes and interfaces retains stable polarization in a $BaTiO_3$ thin film down to the thickness of 0.8 nm. It is found that the polarization could modify the effective potential barrier through the depolarizing filed, indicating that the polarization is possible to control the tunneling conductance of A-FTJ. The coupling among the ionic displacement, spontaneous polarization, and electric field in ferroelectric barrier provides us with multiple degrees of freedom to control the electron transport properties in the A-FTJ. These results reveal the prospective future of the sensitive control of the ferroelectric nanodevices based on A-FTJ.

ACKNOWLEDGMENTS

Helpful discussion with G. H. Zhang is gratefully acknowledged. We also acknowledge the financial support of the National Natural Science Foundation of China (NSFC) 10902128, 11072271, 51172291, 10972239), the Fundamental Research Funds for the Central Universities, New Century Excellent Talents in University, Research

Fund for the Doctoral Program of Higher Education and Fok Ying Tung Education Foundation.

[1]M. N. Baibich, J. M. Broto, A. Fert, F. Nguyen Van Dau, F. Petroff, P. Eitenne, G. Creuzet, A. Friederich, and J. Chazelas, Phys. Rev. Lett. **61**, 2472 (1988).
[2]G. Binash, P. Grünberg, F. Saurenbach, and W. Zinn, Phys. Rev. B **39**, 4828–4830 (1989).
[3]W. Lee, H. Han, A. Lotnyk, M. A. Schubert, S. Senz, M. Alexe, D. Hesse, S. Baik, and U. Gösele, Nat. Nanotechnol. **3**, 402 (2008).
[4]P. R. Evans, X. H. Zhu, P. Baxter, M. McMillen, J. McPhillips, F. D. Morrison, J. F. Scott, R. J. Pollard, R. M. Bowman, and J. M. Gregg, Nano Lett. **7**, 1134 (2007).
[5]E. Y. Tsymbal and H. Kohlstedt, Science **313**, 181 (2006).
[6]G. Gerra, A. K. Tagantsev, and N. Setter, Phys. Rev. Lett. **98**, 207601 (2007).
[7]P. Ghosez and J. Junquera, "First-principles modeling of ferroelectric oxide nanostructures," in *Handbook of Theoretical and Computational Nanotechnology*, edited by M. Rieth, and W. Schommers (American Scientific, 2006), Vol. 7.
[8]J. Junquera and P. Ghosez, Nature **422**, 506 (2003).
[9]A. K. Tagantsev, G. Gerra, and N. Setter, Phys. Rev. B **77**, 174111 (2008).
[10]T. Tybell, C. H. Ahn, and J. M. Triscone, Appl. Phys. Lett. **75**, 856 (1999).
[11]C. H. Ahn, K. M. Rabe, and J. M. Triscone, Science **303**, 488 (2004).
[12]M. Dawber, K. M. Rabe, and J. F. Scott, Rev. Mod. Phys. **77**, 1083 (2005).
[13]D. D. Fong, G. B. Stephenson, S. K. Streiffer, J. A. Eastman, O. Auciello, P. H. Fuoss, and C. Thompson, Science **304**, 1650 (2004).
[14]P. Aguado-Puente and J. Junquera, Phys. Rev. Lett. **100**, 177601 (2008).
[15]V. Garcia, S. Fusil, K. Bouzehouane, S. Enouz-Vedrenne, N. D. Mathur, A. Barthélémy, and M. Bibes, Nature **460**, 81 (2009).
[16]V. Garcia, M. Bibes, L. Bocher, S. Valencia, F. Kronast, A. Crassous, X. Moya, S. Enouz-Vedrenne, A. Gloter, D. Lmhoff, C. Deranlot, N. D. Mathur, S. Fusil, K. Bouzehouane, and A. Barthélémy, Science **327**, 1106 (2010).
[17]C. Ederer and N. A. Spaldin, Phys. Rev. Lett. **95**, 257601 (2005).
[18]J. H. Lee and K. M. Rabe, Phys. Rev. Lett. **104**, 207204 (2010).
[19]C. J. Fennie and K. M. Rabe, Phys. Rev. Lett. **97**, 267602 (2006).
[20]D. D. Fong, A. M. Kolpak, J. A. Eastman, S. K. Streiffer, P. H. Fuoss, G. B. Stephenson, C. Thompson, D. M. Kim, K. J. Choi, C. B. Eom, I. Grinberg, and A. M. Rappe, Phys. Rev. Lett. **96**, 127601 (2006).
[21]Y. Zheng, C. H. Woo, and B. Wang, Nano. Lett. **8**, 3131 (2008).
[22]M. Y. Zhuravlev, R. F. Sabirianov, S. S. Jaswal, and E. Y. Tsymbal, Phys. Rev. Lett. **94**, 246802 (2005).
[23]H. Kohlstedt, N. A. Pertsev, J. R. Contreras, and R. Waser, Phys. Rev. B **72**, 125341 (2005).
[24]P. Maksymovych, S. Jesse, P. Yu, R. Ramesh, A. P. Baddorf, and S. V. Kalinin, Science **324**, 1421 (2009).
[25]M. Stengel, D. Vanderbilt, and N. A. Spaldin, Nature Mater. **8**, 392 (2009).
[26]Y. Zheng, B. Wang, and C. H. Woo, Appl. Phys. Lett. **89**, 083115 (2006).
[27]O. Diéguez, S. Tinte, A. Antons, C. Bungaro, J. B. Neaton, K. M. Rabe, and D. Vanderbilt, Phys. Rev. B **69**, 212101 (2004).
[28]M. E. Lines and A. M. Glass, *Principles and Applications of Ferroelectrics and Related Materials* (Clarendon Press Oxford, 1977).
[29]X. Fang and T. Kobayashi, Appl. Phys. A **69**, S587 (1999).
[30]S. M. Sze and K. K. Ng, *Physics of Semiconductor Devices* (Wiley, Hoboken, NJ, 2007).
[31]N. A. Pertsev and H. Kohlstedt, Phys. Rev. Lett. **98**, 257603 (2007).
[32]Y. Zheng, M. Q. Cai and C. H. Woo, Acta Mater, **58**, 3050 (2010); Y. Zheng, W. J. Chen, C. H. Woo, and B. Wang, J. Phys. D: Appl. Phys. **44**, 095401 (2011).
[33]M. Gajdoš, K. Hummer, G. Kresse, J. Furthmüller, and F. Bechstedt, Phys. Rev. B **73**, 045112 (2006).
[34]W. Zhong, R. D. King-Smith, and D. Vanderbilt, Phys. Rev. Lett. **72**, 3618 (1994).
[35]P. Ghosez, E. Cockayne, U. V. Waghmare, and K. M. Rabe, Phys. Rev. B **60**, 836 (1999).
[36]J. Junquera and P. Ghosez, J. Comput. Theor. Nanosci. **5**, 2071 (2008).
[37]S. L. Dudarev, G. A. Botton, S. Y. Savrasov, C. J. Humphreys, and A. P. Sutton, Phys. Rev. B **57**, 1505 (1998).
[38]G. Gerra, A. K. Tagantsev, N. Setter, and K. Parlinski, Phys. Rev. Lett. **96**, 107603 (2006).
[39]M. Büttiker, Phys. Rev. Lett. **57**, 1761 (1986).
[40]X. Luo, B. Wang, and Y. Zheng, ACS Nano **5**, 1649 (2011); Y. Zheng and C. H. Woo, Nanotechnology **20**, 075401 (2009).
[41]G. Kresse and J. Furthmuller, J. Comput. Mater. Sci. **6**, 15 (1996).
[42]P. E. Blöchl, Phys. Rev. B **50**, 17953 (1994).
[43]M. Brandbyge, J. Mozos, P. Ordejón, J. Taylor, and K. Stokbro, Phys. Rev. B **65**, 165401 (2002).
[44]J. L. Servoin, F. Gervais, A. M. Quittet, and Y. Luspin, Phys. Rev. B **21**, 2038–2041 (1980).
[45]J. W. Edwards, R. Speiser, and H. L. Johnston, J. Am. Chem. Soc. **73**, 2934 (1951).
[46]G. H. Kwei, A. C. Lawson, S. J. L. Billinge, and S. W. Cheong, J. Phys. Chem. **97**, 2368 (1993).
[47]S. H. Wemple, Phys. Rev. B **2**, 2679 (1970).
[48]W. J. Merz, Phys. Rev. **91**, 513–517 (1953).